Crushing Performance and Deformation Mechanics of Additively Manufactured Single-Cell Continuous Basalt Fiber/Polylactic Acid Thin-Walled Tubes

Mohammad Nowfel Mahiuddin [1], Prasenjit Chatterjee [2]

[1] Department of Mechanical Engineering, Lincoln University College, 47301 Petaling Jaya, Malaysia;

[2] Department of Mechanical Engineering, MCKV Institute of Engineering, Howrah, West Bengal - 711204, India.

Email ID: pdf.nowfelmahiuddin@lincoln.edu.my[1]
chatterjee.drprasenjit@gmail.com[2]

Abstract: This paper investigates the quasi-static crushing behavior and progressive deformation modes of 3D-printed continuous basalt fiber-reinforced polylactic acid (CBF-PLA) single-cell thin-walled profiles. By isolating cross-sectional geometries (circular, triangular, square, pentagonal, and hexagonal) and material extrusion rates (E = 0.9, 1.0, 1.1), we demonstrate how corner-driven boundary constraints dictate stability and energy dissipation. Quasi-static axial compression tests reveal a profound geometric dependency: conventional circular tubes succumb to early global Euler buckling, resulting in sudden collapse and poor crush force efficiency (42%). In contrast, multi-sided polygonal geometries promote stable, progressive concertina folding by redistributing localized stresses to corner hinges. Hexagonal profiles exhibited the most stable progressive folding mode, achieving a 22.5% increase in total energy absorption (127.05 J) and a 36.1% improvement in specific energy absorption (5.71 J/g) over circular baselines at E = 1.0. Increasing the extrusion rate to 1.1 enhances fiber deposition density, pushing the hexagonal specific energy absorption to 7.04 J/g, but significantly spikes peak crushing forces by 48.4%. These findings establish topological design as a primary lever for customizing crashworthiness in printed sustainable composites.

Keywords: Continuous basalt fiber, Additive manufacturing, Thin-walled structures, Crashworthiness, Deformation mechanics.

---

1. Introduction

Modern vehicle and aerospace engineering depends heavily on deformable crash structures designed to protect occupants during impacts. Placed strategically behind front bumpers, crash boxes serve as sacrificial components, converting kinetic energy into mechanical deformation before it reaches the passenger cabin. Historically, these structures are fabricated from metals and synthetic fiber-reinforced thermosets, which require specialized, expensive, and inflexible molds. Material extrusion additive manufacturing (ME-AM), particularly fused filament fabrication (FFF), has emerged as a promising alternative, enabling the rapid prototyping and direct fabrication of complex thin-walled profiles without geometric constraints [1]. However, neat polymers and short fiber-reinforced thermoplastic filaments display poor tensile strength and brittle failure mechanisms, restricting their structural use in load-bearing applications. To bypass this bottleneck, co-extruding continuous fiber bundles with a thermoplastic matrix achieves high specific strength and predictable progressive collapse profiles.

Continuous basalt fiber represents an exceptionally sustainable and robust candidate for composite reinforcement. Sourced entirely from natural volcanic mineral rocks melted at approximately 1500 °C, basalt fiber avoids the energy-intensive and toxic chemical synthesis associated with carbon fiber production, presenting a negligible environmental footprint [2]. With a tensile modulus of approximately 80 to 90 GPa and a tensile strength of 2.8 to 3.1 GPa, basalt fiber behaves as a high-performance 'Goldilocks' material, matching the mechanical properties of E-glass while providing superior thermal and chemical resistance. When co-extruding basalt fibers with a biodegradable polylactic acid (PLA) matrix, the solid mechanics of consolidation are governed by the interfacial bonding and the physical placement of the tow. Because continuous fibers are highly rigid, forcing the filament bundle around sharp corners causes severe fiber dragging and corner-cutting defects [3]. These defects are driven by centripetal forces and nozzle dragging transients, leading to matrix-rich pockets and microscopic void zones that degrade structural integrity.

Our central hypothesis is that the cross-sectional geometry of the tube, specifically the corner count and resulting panel intersection angles, governs the transition between unstable buckling and progressive folding. Circular tubes, having no geometric discontinuities to localize stress, buckle globally under axial loads. Conversely, polygonal profiles introduce corner intersections that act as structural hinges, triggering localized progressive plastic collapse (concertina folding) that steadily dissipates impact energy. To preserve unique data for subsequent publications on multi-cell designs and global rate optimizations, this paper isolates the mechanical performance of single-cell hollow thin-walled composite profiles. By evaluating collapse modes and crashworthiness metrics under quasi-static axial compression, we map how geometric design and extrusion rates combine to dictate structural energy absorption.

2. Experimental Methodology

Continuous basalt fiber tows (filament diameter of 13 µm, density of 2.65 g/cm^3, tensile strength of 3000 MPa, and tensile modulus of 90 GPa) were obtained from Jilin Tong Xin Basalt Technology Co., Ltd. Biodegradable PLA filament (eSUN, 1.75 mm diameter) was used as the thermoplastic matrix. Fabrication was conducted on a customized Ender3 V2 desktop 3D printer retrofitted with an in-nozzle impregnation co-extrusion printhead. This setup heats and consolidates the PLA and CBF in a single melt zone immediately before deposition. Specimens were printed flat with a 0° raster orientation, 100% infill, and a single-layer skirt, completely omitting neat polymer outer shells to ensure a uniform composite core.

The experimental framework utilized a two-factor full factorial Design of Experiments (DOE): Cross-sectional Geometry (circular, triangular, square, pentagonal, and hexagonal) and Material Extrusion Rate (E = 0.9, 1.0, and 1.1). To ensure an unbiased topological comparison, the total cross-sectional area of the solid wall was held constant at approximately 12.6 mm^2 across all geometries, while the wall thickness (t = 1.9 mm) and tube height (H = 90 mm) were kept uniform. Dimensions were: circular diameter D = 50 mm, triangular side LT = 33 mm, square side LQ = 25 mm, pentagonal side LP = 30 mm, and hexagonal side LH = 25 mm. Baseline print parameters were optimized at a nozzle temperature of 195 °C, a print speed of 100 mm/min, and a layer thickness of 0.25 mm to maximize interlayer bonding.

The rigid nature of basalt fiber presents a significant geometric challenge during printing, as it resists bending and cuts sharp corners. This 'corner-cutting' effect creates a trajectory deviation (δ) between the actual deposition path and the intended G-code, resulting in matrix-starved voids [4]. To solve this, toolpath corner smoothing was evaluated. We found that rounding G-code corners with a radius of R = 1 mm reduced the corner deviation δ by 39.9% (from 2.16 mm to 1.30 mm) under identical printing settings. While a tighter radius failed to hold the fiber, an overly large radius (R = 3 mm) caused significant dimensional distortion. Consequently, a path smoothing filter of R = 1 mm to R = 2 mm was applied to all polygonal toolpaths to ensure dimensional fidelity.

Quasi-static axial compression testing was performed on an MTS universal testing machine at room temperature. Specimens were compressed between flat steel platens at a constant crosshead speed of 10 mm/min up to a total displacement of 60 mm (exactly two-thirds of the specimen height). Raw load-displacement history was sampled at 500 Hz. Five solid mechanics metrics were extracted: Total Energy Absorption (EA, J), Specific Energy Absorption (SEA, J/g, computed as EA divided by mass), Peak Crushing Force (PCF, kN), Mean Crushing Force (MCF, kN), and Crush Force Efficiency (CFE = MCF/PCF, expressed as a percentage). A minimum of three replicates were tested for each experimental design point to ensure statistical reproducibility.

3. Results and Discussion

3.1 Deformation Mechanics and Collapse Modes

The experimental results demonstrate a clear bifurcation in collapse modes dictated by cross-sectional topology. At the nominal extrusion rate (E = 1.0), the circular specimen (C2) failed through sudden global Euler buckling. Upon loading, the circular tube reached a peak crushing force (PCF) of 3.88 kN, followed immediately by lateral column instability. The tube bowed outward, causing severe horizontal matrix cracking and catastrophic failure without forming successive folds. Consequently, its crushing force plunged to a low mean of 1.64 kN, yielding a Crush Force Efficiency (CFE) of only 42% and a specific energy absorption (SEA) of 4.19 J/g. This global buckling represents an unfavorable collapse mode since a large volume of the composite escapes plastic deformation, significantly reducing total energy dissipation.

In contrast, the polygonal geometries successfully bypassed global column instability, collapsing via stable, progressive concertina folding. Here, the sharp panel intersections function as longitudinal structural hinges, concentrating plastic strain and guiding the adjacent flat faces into symmetric, accordion-like folds. The hexagonal tube (H2) exhibited the most stable collapse profile. It reached a PCF of 3.69 kN and maintained a remarkably high mean crushing force (MCF = 2.12 kN), resulting in a CFE of 57%. This stable progressive collapse is visually reflected in the force-displacement traces shown in Figure 1, where the hexagonal curve exhibits uniform load oscillations corresponding to the successive formation of plastic folding hinges, contrasting sharply with the immediate load drop of the circular tube. At the nominal extrusion rate, the hexagon absorbed 127.05 J of total energy, outperforming the circular tube by 22.5% in total EA and achieving an SEA of 5.71 J/g, which is comparable to hexagonal structures reported in literature [5].

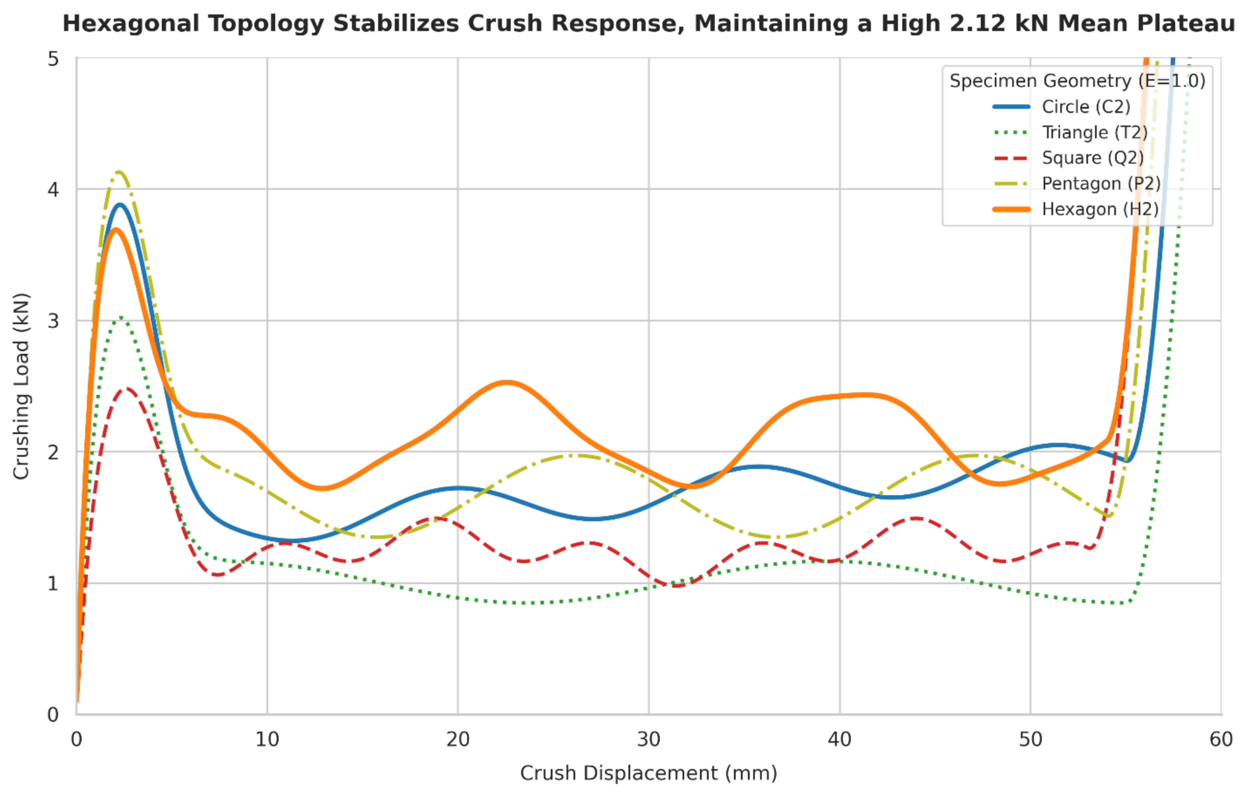

Figure 1. Experimental axial force versus displacement responses for single-cell CBF-PLA tubes under nominal extrusion (E = 1.0), showing the high-amplitude load plunge of circular columns compared to the stable progressive load oscillations of polygonal geometries.

The other polygonal profiles showed intermediate deformation modes. The triangular profile (T2) concentrated substantial compressive stress at its acute 60° corners, triggering rapid local fracturing and fiber splitting. This local fracture propagated vertically, leading to premature global tilting and yielding a low CFE of 35% and an SEA of 3.89 J/g. The square tube (Q2) formed a stable, progressive fold sequence but suffered from lower sustained load due to its wider, less constrained flat walls, resulting in a modest SEA of 3.62 J/g. The pentagonal tube (P2) demonstrated highly competitive performance, reaching the highest PCF of 4.13 kN and collapsing with a stable force plateau, achieving an EA of 105.64 J and an SEA of 5.59 J/g. These behaviors highlight that incorporating multi-sided topologies serves as a powerful energy-absorption mechanism, consistent with hybrid fiber designs [6] and sustainable transportation crash boxes [7].

3.2 Material Extrusion Rate Dependency

While cross-sectional geometry dictates the primary collapse mode, the material deposition rate dramatically shifts the energy absorption capacity of the printed walls. The extrusion multiplier (E) controls the volume and density of the PLA matrix relative to the continuous fiber tow. At a low extrusion rate of E = 0.9, the composite walls suffer from matrix starvation. This insufficient polymer volume leaves high microscopic void fractions and weak interlayer bonding, which manifests as severe horizontal delamination, fiber pull-out, and matrix cracking under axial loading. The lack of lateral matrix support allows individual basalt fiber strands to buckle locally, degrading load retention. For instance, the hexagonal tube H1 (E = 0.9) achieved a total energy absorption of only 90.19 J and an SEA of 4.38 J/g.

Conversely, raising the extrusion rate to E = 1.1 significantly enhances mechanical performance. The high extrusion multiplier increases deposition pressure within the nozzle, squeezing out microscopic voids and maximizing interlaminar shear strength. This robust consolidation locks the rigid continuous basalt fiber bundles in place, enabling effective interlaminar stress transfer and activating fiber-bridging mechanisms that delay crack propagation. This behavior is analyzed in Figure 2, which demonstrates the influence of extrusion rates on Specific Energy Absorption and Peak Crushing Force. At E = 1.1, the hexagonal profile (H3) achieves an outstanding SEA of 7.04 J/g, representing a 23.4% increase over its nominal counterpart (5.71 J/g). This trend aligns with microstructural void control models [8]. However, over-extrusion causes a severe 48.4% spike in PCF, surging the hexagon's peak force from 3.69 kN to 5.47 kN. In active vehicles, such a spike would cause dangerous deceleration pulses, undermining passenger safety. Furthermore, E = 1.1 increases filament consumption, validating the selection of E = 1.0 as the optimal operational window.

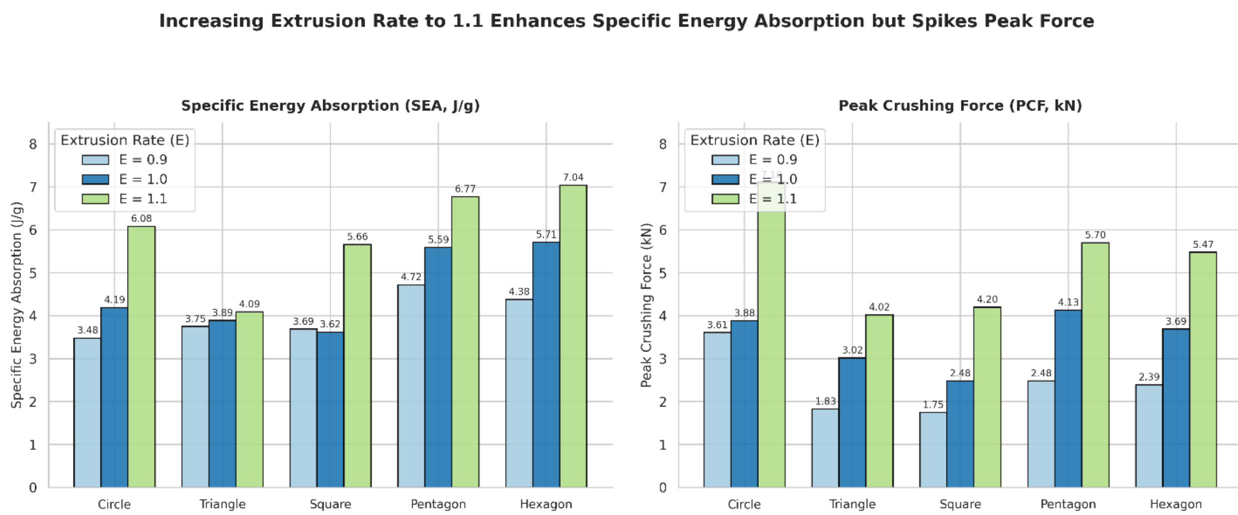

Figure 2. Scaling effects of material extrusion rate (E = 0.9, 1.0, 1.1) on (a) Specific Energy Absorption (SEA) and (b) Peak Crushing Force (PCF) across all geometries, highlighting the load escalation associated with dense consolidation.

3.3 Solid Mechanics of Multi-Sided Topologies

The physical mechanics behind the superiority of multi-sided polygonal profiles are governed by the panel intersection angles. As the side count increases from three to six, the internal intersection angle between adjacent flat faces becomes increasingly obtuse (60° for a triangle, 90° for a square, 108° for a pentagon, and 120° for a hexagon). A highly obtuse angle significantly reduces the stress concentration factor at the corner. Furthermore, the obtuse corner reduces the commanded path curvature during G-code slicing, lowering the centripetal force required to deposit the fiber tow. As defined by our printable-curvature governing mechanics, a lower curvature requirement prevents corner-cutting, enabling the continuous fiber to follow the commanded path with high fidelity [9]. This high-fidelity placement guarantees that continuous basalt fibers are aligned precisely along the high-stress corner zones, where they bridge micro-cracks and sustain post-peak load-carrying capacity.

Additionally, increasing the corner count increases the number of localized plastic hinges per unit volume, which effectively shortens the folding wavelength. This higher hinge density forces the composite to deform through multiple compact, high-frequency folds rather than a few large, unstable folds. This solid mechanics relationship is visualized in the crashworthiness performance map in Figure 3. The chart maps SEA against CFE, showing that the hexagonal (H2) and pentagonal (P2) profiles sit comfortably in the optimal upper-right quadrant, representing high energy absorption capacity combined with low deceleration risks. Conversely, triangular and circular profiles occupy the unfavorable lower-left regions due to unstable buckling and local fracturing, confirming that topology acts as a highly effective control lever for tuning crash performance [10].

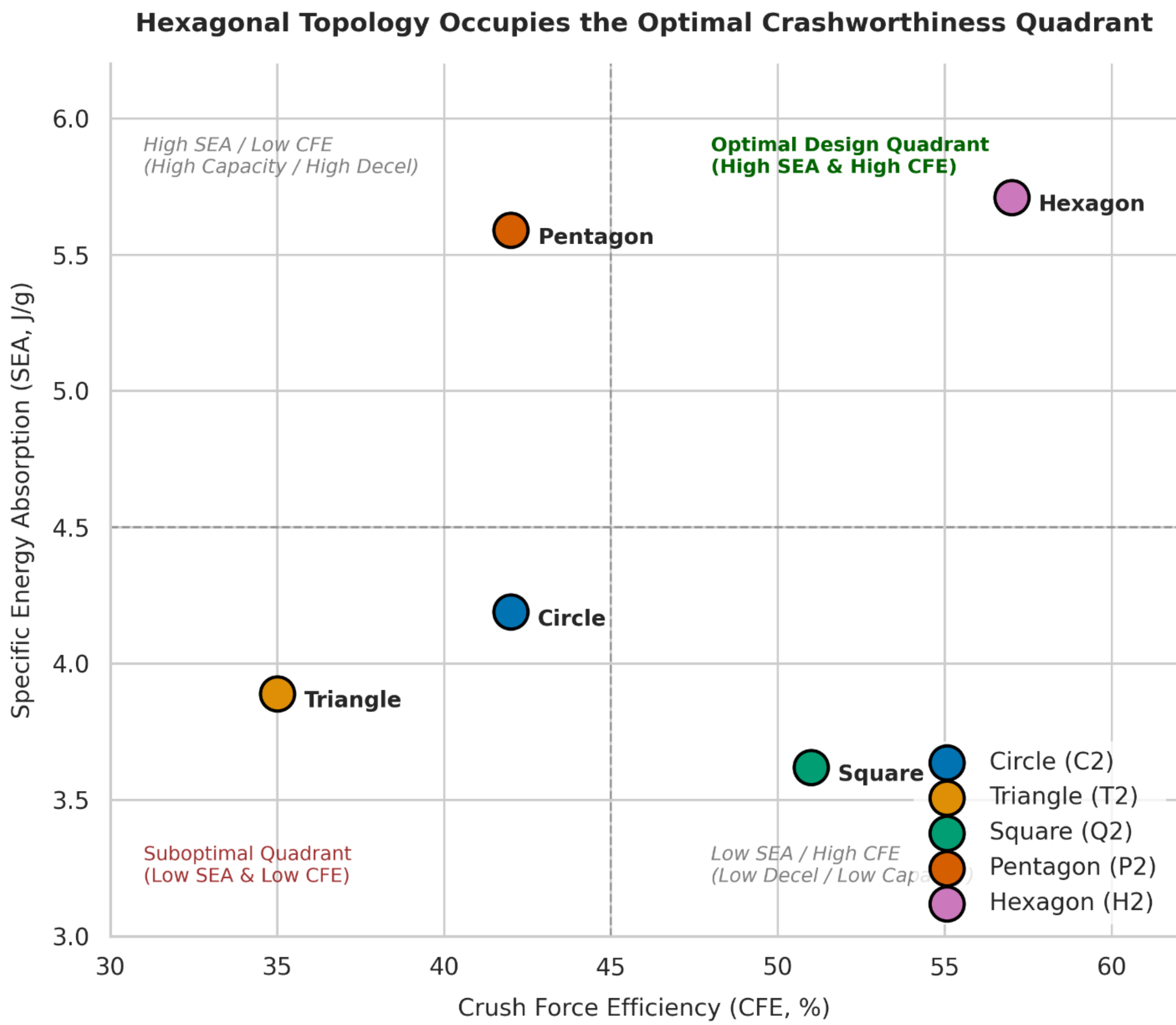

Figure 3. Specific Energy Absorption (SEA) versus Crush Force Efficiency (CFE) trade-off map for the single-cell tubes at nominal extrusion (E = 1.0), illustrating the functional superiority of hexagonal and pentagonal topologies in the design space.

To provide a complete numeric reference of the experimental program, Table 1 compiles the crashworthiness performance indicators across all cross-sections and extrusion multipliers. This unified dataset highlights how geometry governs the primary collapse mechanism, while the extrusion multiplier acts as a secondary density-reinforcement knob.

Table 1. Quantitative crashworthiness indicators of 3D-printed single-cell CBF-PLA thin-walled tubes.

Specimen	Extrusion (E)	EA (J)	Mass (g)	SEA (J/g)	PCF (kN)	CFE (%)
C1 (Circle)	0.9	75.04	21.57	3.48	3.61	34%
C2 (Circle)	1.0	98.40	23.48	4.19	3.88	42%
C3 (Circle)	1.1	143.59	23.61	6.08	7.10	34%
H1 (Hexagon)	0.9	90.19	20.59	4.38	2.39	62%
H2 (Hexagon)	1.0	127.05	22.26	5.71	3.69	57%
H3 (Hexagon)	1.1	169.96	24.13	7.04	5.47	52%
Q1 (Square)	0.9	70.93	19.20	3.69	1.75	68%
Q2 (Square)	1.0	76.05	20.99	3.62	2.48	51%
Q3 (Square)	1.1	129.26	22.85	5.66	4.20	51%
T1 (Triangle)	0.9	56.66	15.12	3.75	1.83	51%
T2 (Triangle)	1.0	64.37	16.51	3.89	3.02	35%
T3 (Triangle)	1.1	73.06	17.84	4.09	4.02	30%
P1 (Pentagon)	0.9	81.53	17.29	4.72	2.48	54%
P2 (Pentagon)	1.0	105.64	18.87	5.59	4.13	42%
P3 (Pentagon)	1.1	139.46	20.62	6.77	5.70	40%

4. Conclusions

This research has systematically characterized the quasi-static axial crushing behavior and progressive failure mechanics of 3D-printed continuous basalt fiber-reinforced PLA thin-walled tubes. The experimental results lead to the following conclusions:

1. Cross-sectional topology directly dictates the primary collapse mechanism. Circular geometries succumb to early global Euler buckling (CFE = 42%, SEA = 4.19 J/g), whereas polygonal shapes promote progressive concertina folding by forming localized plastic hinges.
2. The hexagonal configuration is the superior single-cell hollow topology. Under nominal settings (E = 1.0), the hexagon absorbs 127.05 J of total energy (yielding an SEA of 5.71 J/g), outperforming the circular tube by 22.5% in total EA and providing a stable force plateau with a CFE of 57%.

3. Material extrusion rates strongly influence matrix consolidation and interlaminar bonding. Raising the extrusion rate to E = 1.1 increases composite compaction and raises the hexagon's specific energy absorption to 7.04 J/g. However, this causes a severe 48.4% spike in PCF, verifying that E = 1.0 represents the optimal engineering balance.

References

1. R. Matsuzaki, M. Ueda, M. Namiki, T. K. Jeong, H. Asahara, K. Horiguchi, T. Nakamura, A. Todoroki, and Y. Hirano, "Three-dimensional printing of continuous-fiber composites by in-nozzle impregnation," Sci. Rep., vol. 6, p. 23058, 2016. DOI: 10.1038/srep23058.
2. V. Fiore, T. Scalici, G. Di Bella, and A. Valenza, "A review on basalt fiber and its composites," Compos. Part B Eng., vol. 74, pp. 74-94, 2015. DOI: 10.1016/j.compositesb.2014.12.006.
3. W. Zhu et al., "Three-dimensional printing of high-performance continuous fiber-reinforced thermoplastic composites: Causes and elimination of process-induced defects," Compos. Part B Eng., vol. 292, p. 112080, 2025. DOI: 10.1016/j.compositesb.2024.112080.
4. O. A. Mohamed, S. H. Masood, and J. L. Bhowmik, "Modeling, analysis, and optimization of dimensional accuracy of FDM-fabricated parts using definitive screening design and deep learning feedforward artificial neural network," Adv. Manuf., vol. 9, pp. 115-129, 2021. DOI: 10.1007/s40436-020-00336-9.
5. M. F. M. Alkbir, S. B. Mohamed, S. M. Sapuan, and A. Endut, "Experimental studies on crushing behaviour of hexagonal composite tubes," J. Text. Eng. Fashion Technol., vol. 3, no. 1, pp. 557-559, 2017. DOI: 10.15376/biores.19.2.3106-3120.
6. P. R. Govindarajan, R. Shanmugavel, S. Palanisamy, T. Khan, and O. S. Ahmed, "Crash-worthiness analysis of hollow hybrid structural tubes (aluminum mesh with basalt-bamboo composite) by roll wrapping," BioResources, vol. 19, no. 2, pp. 3106-3120, 2024. DOI: 10.15376/biores.19.2.3106-3120.
7. S. Samim and M. Mustapha, "Advancements in fiber-reinforced composite tubes for energy absorption and automotive crashworthiness: a greener outlook," Emerg. Mater., vol. 8, no. 6, pp. 4007-4035, 2025. DOI: 10.1007/s42247-025-01091-y.
8. R. Viano, L. Demont, P. Margerit, R. Mesnil, J.-F. Caron, and D. Weisz-Patrault, "Residual stress control in large-format additive manufacturing of polylactic acid via a digital twin and in-operando imaging," Mater. Des., vol. 260, p. 114870, 2025. DOI: 10.1016/j.matdes.2025.114870.
9. M. Liu, S. Qu, S. Li, X. Yan, W. Li, and Y. Wang, "Modeling and compensation methods for trajectory errors in continuous fiber-reinforced thermoplastic composites using 3D printing," Polymers, vol. 17, no. 13, p. 1865, 2025. DOI: 10.3390/polym17131865.
10. X. Chi, J. Xue, L. Jia, J. Yao, H. Miao, L. Wu, T. Liu, X. Tian, and D. Li, "Machine learning-based online monitoring and closed-loop controlling for 3D printing of continuous fiber-reinforced composites," Addit. Manuf. Front., vol. 4, no. 2, p. 200196, 2025. DOI: 10.1016/j.amf.2025.200196.